The Outcome of Bisphosphonate-Related Osteonecrosis of the Jaw Patients' Gingiva-Derived Mesenchymal Stem Cells on Wound Healing in a Mice Excisional Skin Model.

Mengyu Li
Shanghai 9th Peoples Hospital Affiliated to Shanghai Jiaotong University School of Medicine
Yejia Yu
Shanghai 9th Peoples Hospital Affiliated to Shanghai Jiaotong University School of Medicine
Jiajia Wang
Shanghai 9th Peoples Hospital Affiliated to Shanghai Jiaotong University School of Medicine
Yuqiong Zhou
Shanghai 9th Peoples Hospital Affiliated to Shanghai Jiaotong University School of Medicine
Yueqi Shi
Shanghai 9th Peoples Hospital Affiliated to Shanghai Jiaotong University School of Medicine
Wenjie Zhang
Shanghai 9th Peoples Hospital Affiliated to Shanghai Jiaotong University School of Medicine
Geehun Son
Shanghai 9th Peoples Hospital Affiliated to Shanghai Jiaotong University School of Medicine
Jing Ge
Shanghai 9th Peoples Hospital Affiliated to Shanghai Jiaotong University School of Medicine
Jun Zhao
Shanghai 9th Peoples Hospital Affiliated to Shanghai Jiaotong University School of Medicine
Zhiyuan Zhang
Shanghai 9th Peoples Hospital Affiliated to Shanghai Jiaotong University School of Medicine
Chi Yang
Shanghai 9th Peoples Hospital Affiliated to Shanghai Jiaotong University School of Medicine
Shaoyi Wang (wangshaoyi163@163.com)
Shanghai Ninth People's Hospital, Shanghai Jiao Tong University School of Medicine
https://orcid.org/0000-0002-0871-9584

Research

Keywords: Bisphosphonates, Osteonecrosis, Gingival mesenchymal stem cells, Transplantation, Wound healing, Microenvironment, Oral mucosa

Posted Date: January 7th, 2021

DOI: https://doi.org/10.21203/rs.3.rs-139953/v1

Abstract

Background: Retarded gingival healing is the hallmark of bisphosphonate-related osteonecrosis of the jaw (BRONJ) and poses a great challenge to maxillofacial surgeons. Although previous studies have showed that bisphosphonates (BPs) are highly toxic to healthy gingival mesenchymal stem cells (GMSCs) in vitro, there is overall lack of direct evidence demonstrating the regeneration capacity of oral mucosa in BRONJ patients. In present study, we aim to isolate GMSCs from BRONJ patients' gingiva and assessed their phenotypes and functions in vitro, as well as their therapeutic effects for wound healing in a mice excisional skin model.

Methods: BRONJ patients' gingival samples were used for microarray analysis, histological detection and cell culture. The stem cells isolated from the central gingiva (center-BRONJ GMSCs) and the peripheral lesions (peri-BRONJ GMSCs) were analyzed by Cell Counting Kit-8 (CCK-8), cell adhesion, scratch and flow cytometry. Luciferase/GFP (Green Fluorescent Proteins)-labeled GMSCs combined with Hydrogel were transplanted in a mice excisional skin model, and mice were divided into a hydrogel alone group, a hydrogel/control GMSCs group, a hydrogel/center-BRONJ GMSCs group and a hydrogel/peri-BRONJ GMSCs group. Bioluminescence imaging trace cell survival in vivo. Healing effects were evaluated by wound area measurement, histology, immunohistochemistry (IH) and immunofluorescence (IF).

Results: Center-BRONJ GMSCs and peri-BRONJ GMSCs were all fibroblast-like cells, but they became slender and more wrinkled compared control GMSCs. Notably, they exhibited decreased proliferation, adhesion, migration capacities and underwent early apoptosis in vitro. In animal model, BRONJ GMSCs transplantation also displayed lower cell survival rate and poor healing effects than that of control group. Mechanistically, we found that the expression of TGF-β1 signaling pathway was suppressed not only in BRONJ patients' gingival lesions but also in BRONJ GMSCs transplantation animal model.

Conclusions: In BRONJ patients' microenvironment, the regeneration ability of oral mucosa was dramatically decreased. Our mice skin model demonstrated for the first time that BRONJ GMSCs transplantation displayed poor effects on wound healing mainly via suppressing TGF-β1 signaling pathway. This study provides new insights into the prevention for BRONJ by improving the functions of GMSCs in accelerating gingival wound healing.

Background

Bisphosphonate-related osteonecrosis of the jaw (BRONJ) is a detrimental side effect that specifically occurs in the oral cavity in cancer patients receiving high doses of intravenous bisphosphonates (BPs), severely affecting patients' quality of life (1). The hallmark of BRONJ are necrotic bone exposure and retarded gingival healing, however, it is unclear why such the lesion should present with soft tissue defects as the primary clinical feature and the underlying mechanism is still largely unknown(2).

Previously, we observed that BRONJ patients displayed cracked, edematous periodontal ligament fibers (3). In the present study, we further found that BRONJ patients' gingiva also appeared as disordered

lamina propria and displayed notably depressed expressions of collagen. In comparison to other parts of the human body, oral mucosa is a unique tissue that directly links with the underlying bone and external bacterial environment, which is easily damaged by jaw trauma, especially tooth extraction and alveolar surgery (4). In clinical, approximately 80% of BRONJ cases was due to long-term mucosal nonunion after invasive dental procedures (5). Recent research also suggested that poor gingival wound healing after tooth extraction in patients treated with BPs increases the susceptibility to bacterial infection, contributing to the development of BRONJ (6, 7). Therefore, it is extremely urgent to explore the microenvironment of BRONJ patients' oral mucosa and look for new therapeutic methods to promote gingival wound healing. Gingival mesenchymal stem cells (GMSCs) are a group of stem cells isolated from the gingival lamina propria, and perform remarkable tissue regenerative potential and noteworthy immunomodulatory properties (8). Previous studies have showed that BPs inhibited healthy GMSCs viability and fibrogenesis in vitro (5, 9–11), however, there is a lack of direct evidence demonstrating the regeneration capacity of oral mucosa in BRONJ patients.

In this study, to embark on exploring the regeneration capacity of oral mucosa and the exact mechanism of BRONJ, firstly, we performed a microarray analysis using gingival tissues obtained from BRONJ patients or healthy people and explored differentially regulated genes. Secondly, we isolated GMSCs from the central lesions (center-BRONJ GMSCs) and the peripheral area of BRONJ patients' gingiva (peri-BRONJ GMSCs) respectively. After that, we compared their proliferation, adhesion, migration, apoptosis in vitro and their therapeutic effects for the treatment of wound healing in a mice excisional skin model. We anticipate the study will generate fresh insight into the underlying mechanism of BRONJ and suggest the important ramifications in the prevention and treatment for BRONJ.

Methods And Materials

Sample Collection

Five BRONJ patients, ages 54–81 years, underwent surgery at the Department of Oral Surgery, Ninth Peoples Hospital. Debridement of the affected bone and gingiva was extended to reach healthy-appearing tissues (12, 13). BRONJ patients were considered eligible for this study if they had a histologically confirmed advanced solid cancer and radiographic confirmation of bone metastases, receiving intravenous BPs and presented with exposed necrotic bone in the maxillofacial region at least eight. Patients were considered ineligible when they had received any radiotherapy, chemotherapy, immunotherapy, or hormonotherapy before the study. The control group included five patients, older than 50, without bone metabolism diseases. They underwent third molar extraction, meanwhile, gingival tissues surrounding the tooth were collected. All patients provided written informed consent to participate in this study. Detailed patient information is listed in Supplement 1.

cDNA microarray

Gene expression profiling was performed using the Affymetrix GeneChip (Affymetrix, Santa Clara, CA, US). The details of RNA sample extraction and quality control were in Supplement 2. Raw data were

normalized by RMA algorithm, Affymetrix packages in R. Differentially expressed genes were selected at ≥2-fold and $p < 0.005$. Gene Ontology (GO) analysis and Kyoto Encyclopedia of Genes and Genomes (KEGG) analysis were performed using the clusterProfler R/bioconductor package version 3.16.0. Only pathways with ≥2 genes were included in the analysis. P-values of hypergeometric tests were adjusted for multiple testing via the Benjamini-Hochberg method. For all pathways with adjusted P-value ≤0.05.

Histological Analysis

Gingival samples fixed in 4% paraformaldehyde were embedded in paraffin and sliced for histological evaluation. Paraffin sections were stained with hematoxylin and eosin (H&E) as well as Masson staining. For IH staining, after deparaffinization, rehydration, antigen retrieval, permeabilization and blocking non-specific binding, sections were incubated in primary antibodies against collagen type I A1(COLIA1) (Abcam; 1:200), transforming growth factor beta 1 (TGF-β1) (Abcam; 1:300), caspase 3 (Abcam; 1:200) at 4°C overnight and secondary antibodies (Servicebio; 1:500) for 1 hour at room temperature. DAPI (Abcam) at 1:500 was used as nuclear counterstain. Results were detected by fluorescence microscope (Olympus). BRONJ patients' gingival samples were also assessed by TUNEL staining with Cell Death Fluorescein Detection Kit (Roche) following the manufacturer's instructions. The experimental method was conducted as previously reported (3).

Isolation of GMSCs from BRONJ and healthy gingival tissues

GMSCs were isolated from gingiva as previously described (14), GMSCs under 3-5 passages were used. The cell morphology was analyzed with direct microscopic observation and immunofluorescence assay. First, microscopic images of the cells were acquired using an inverted contrast-phase microscope (Nikon, Tokyo, Japan). Then the cells were stained with a fluorescent dye for actin called (Tetramethyl Rhodamine Isothiocynate) TRITC phalloidin (YEASEN, USA). Fluorescence images were obtained using a fluorescence microscope (Olympus, Tokyo, Japan).

Flow Cytometric

Surface antigens of GMSCs were analyzed by flow cytometry. Briefly, 2×10^5 cells were incubated with mouse anti-human CD45, CD31, CD146, CD90 and CD105 for 30 min at 37°C. Labeled cells were analyzed using a flow cytometer (Beckman, USA).

Cell Proliferation, adhesion and scratch Assay

GMSCs were seeded at a density of 3×10^3 cells/mL into 96-well plate. The cell number was assessed on 1,3,5,7 days using Cell Counting Kit-8 (Beyotime) assay. The optical density was measured at 450nm using the Spark™ 10M Multimode Microlpate Reader (TECAN). The experiments of cell adhesion and scratch were done according to previously reported protocol[15]. For cell adhesion, GMSCs were divided into 5.0×10^4 cells/ml and subsequently seeded on to type I collagen coated 6 well plates and incubated for 30 min at 37°C. Then the wells were rinsed vigorously three times with phosphate buffered saline

(PBS), and the remaining cells were stained using 0.1% crystal violet dye. Data were expressed as adherent cells per field. For cell scratch, GMSCs were plated at 200,000 cells/well in 6-well plates. Once confluent, a scratch wound was performed using a sterile 10μl pipette tip. The size of the gap was measured microscopically immediately (0 h) and 24 h later.

Cell Cycle and Apoptosis

GMSCs were seeded at a density of 5×103 cells/ml into 6-well plate. After cell were detached, cell cycle was analyzed using CycleTESTTM PLUS DNA Reagent Kit (BD, Biosciences). After cells were fixed in 75% ice-cold ethanol, cell apoptosis was analyzed using FITC Annexin V Apoptosis Detection Kit I (BD, Biosciences). Finally, the samples were filtered through 22-μm nylon mesh and evaluated by flow cytometer (Beckman, USA).

RT-PCR

Total mRNA was isolated using TRIzol reagent (Invitrogen Life Technologies), cDNA was prepared using GoScript Reverse Transcription System (Promega), and an ABI Prism 7500 (Bioscience) was used to perform quantitative RT-PCR. The relative mRNA expression levels was determined by normalizing to the β-Actin threshold cycle and calculated using the $^{\triangle\triangle}$Ct method. Primers are shown in Supplement 3.

Western Blotting

Proteins were extracted from GMSCs, and Western blot assays were performed as previously described (16). Primary antibodies against β-actin, TGF-β1, COLIA1 and p-Smad3 were used.

In vivo Wound Healing Assay

Lentiviral vector Transduction

Lentiviral vector PCHMWS-GFP-T2A-Fluc was purchased from Dr. A. Ibrahimi (Katholieke Universiteit Leuven). This vector contained a fused gene encoding for the firefly luciferase (Fluc) and GFP. Briefly, GMSCs were plated at 100,000 cells into 25-cm2 flask. After overnight culture, cells were transduced with 2 ml medium that contained lentiviral vector at 37°C for 3-4 hours by the multiplicity of infection (MOI) of 20 and then replaced with fresh medium. Three runs of cell transduction were carried out. Four days after the first transduction, the transduced GMSCs reached confluency and were subcultured at a density of 1000 cells/cm^2 in 150-cm^2 flasks. After 7 days, when these cultures were near confluency, the GMSCs were cryopreserved at 10^6/vial (passage 3) at -80°C. The cells were selected with puromycin (Genomeditech, China) at a low concentration (2 μg /mL) and cultured for 5 days. A GFP-positive signal was detected in 95% of the selected cells under an inverted fluorescence microscope (Nikon, Japan).

In Mice Skin wound healing model

Luciferase/GFP-labeled GMSCs were implanted in wound healing model as described previously (17-19). In brief, 5-week-old immunocompromised mice were individually anesthetized using an intraperitoneal injection of ketamine (75 mg/kg) and rinsed with an alcohol swab and sterilely prepped with betadine and draped. A sterile 8mm diameter full-thickness wound was created on the on the dorsum of the nude. A donut-shaped splint with a 10mm inner diameter and 10mm outer diameter was fashioned from a 0.5 mm-thick silicone sheet (Grace Bio-Laboratories, Bend, OR). An immediate-bonding adhesive (Tegaderm, 3M) was used to fix the splint to the skin followed by interrupted 5–0 nylon (Ethicon, Inc,Somerville, NJ) sutures to ensure position. Mastisol (Fernadale, MI) was applied to the perimeter of the wound to improve adherence of the occlusive dressing (Tegaderm, 3M) placed to cover the wounds. The animals were placed in individual cages under a warming lamp and allowed to recover fully from anesthesia. The wound dressings in each group were changed every 3 days according the above methods. 20 mice were randomly divided into four groups: Group A, hydrogel alone; Group B, hydrogel/control GMSCs; Group C, hydrogel/center-BRONJ GMSCs; Group D, hydrogel/peri-BRONJ GMSCs, n = 5. Figure 5 showed the experimental design and schematic representation of wound healing model in nude mice.

Bioluminescence imaging

On days 7 and 14 post transplantation, in vivo cell viability was confirmed by measuring the luciferase activity with an IVIS bioluminescence imaging system (IVIS Lumina III, PerkinElmer, USA). Briefly, prior to anesthesia, D-luciferin (potassium salt, Yeasen, China) was injected into the mice at 150 mg/kg. The mice were imaged 20 min after injection. Photon flux was measured and quantified by the system software.

Wound closure measurements

Every day, nude mice were observed and digital images were taken. Wound area was measured by tracing the wound margin and calculating the pixel area using Image-J 1.52a software. The wound healing rates were calculated as follows: wound closure rate = (A0 − At)/A0 (20). A0 is the initial wound area, and At is the wound area at 5, 10 and 14 days post-surgery.

Histology

After 2 weeks, all mice were sacrificed and the wound tissues were harvested with a rim healthy normal skin tissue. Tissue samples were fixed in 10 % formalin. Frozen sectioning and fluorescence microscope detected cell viability as described previously (21). After imaging by a fluorescence microscope, five random fields were selected to calculate GFP signal areas. Then, the samples were stained with H&E and Masson staining. The lengths of neo-epithelium in H&E staining were calculated according to previously described methods (20). Masson's staining was used to determine the content and maturity of collagen in the wound beds. The fraction of collagen was calculated by detecting the blue area in five random files under the 400× magnification fields of each group using Image-J 1.52 software. IH staining was the same as the previous experiment.

Statistical Analyses

All statistical analyses were performed using GraphPad Prism 7 (GraphPad Software). The outcome measurements are expressed as the mean±standard deviation. Differences between two groups were analyzed by t-test. $P \leq 0.05$ was considered as the statistically significant difference for all comparisons. All experiments were conducted in triplicate.

Results

Microarray gene profiling identifies the activation of the negative regulation of wound healing and the suppressed TGF-β signaling pathways

To explore the underlying mechanisms of the retarded gingival wound healing in BRONJ patients, we performed an Affymetrix Gene Expression Array analysis using tissues obtained from BRONJ patients or healthy people and explored differentially regulated genes. BRONJ gingival tissues were subjected to microarray profiling, and differentially expressed genes that were either upregulated or downregulated more than threefold were obtained (Fig. 1A). Figure 1B exhibited the top 10 of Gene ontology (GO) enrichment in analysis (22), and we identified “negative regulation of wound healing” as one of the most significantly associated biological process in BRONJ lesions, in which fibroblast growth factor receptor 1 (FGFR1) and Smad3 were all downregulated (Fig. 1D). Kyoto Encyclopedia of Genes and Genomes (KEGG) analysis (23) (Fig. 1C) showed the top 10 of pathway enrichment, in which “TGF-β signaling pathways” as the significantly enriched functional pathway associated with the retarded gingival wound healing in BRONJ patients. Involved in this signaling pathway, expression of COLIA1, COL3A1, COL11A1 and TGF-β1, TGF-β3, Smad3 were highly downregulated (Fig. 1E).

Tgf-β1 Signaling Pathway Was Suppressed In Bronj Patients’ Gingiva

To verify the microarray results, we validated the suppressed expression of TGF-β signaling pathway in BRONJ patients’ gingiva. Figure 2A showed the progressive enlargement of the gingiva defects in a BRONJ patient within 3 months. Gingival samples were assessed following HE staining. In contrast with healthy gingiva, the central and peripheral area of BRONJ gingiva were infiltrated with abundant lymphocyte and plasma cells (yellow arrow), and appeared as irregular, serrated spikes (Fig. 2B). Masson staining displayed the disorganized lamina propria showing cracked, loose and a major reduction of collagen fibers (yellow arrow) in BRONJ gingiva (Fig. 2C). The mRNA levels of BRONJ gingiva were determined by real-time PCR, we found that the expression of TGF-β1, Smad3, COLIA1 but not TGF-β3, Smad2 were remarkably downregulated in BRONJ gingiva (Fig. 1F). The same pattern was further confirmed by immunohistochemical staining, which showed a lower expression of TGF-β1, and COLIA1 in the central and peripheral area of BRONJ sites than that in healthy gingiva (Fig. 2D). Collectively, these data suggest that TGF-β1 signaling pathway is suppressed both in BRONJ gingival tissues.

Isolation of GMSCs from BRONJ patients’ gingiva and healthy gingiva

The stromal cells were derived from gingival tissues in the central area of BRONJ region (center-BRONJ GMSCs), peripheral area (peri-BRONJ GMSCs) and health gingiva (control GMSCs). These cells were all fibroblast-like cells, but the central and peripheral BRONJ GMSCs became slender and more wrinkled, resembling ice crystals (Fig. 3A). Consistent with the microscopic observation, fluorescence images (Fig. 3B) of actin fibers in control GMSCs showed a dense and aligned network-like structure throughout the whole of the cell body, while the central and peripheral BRONJ GMSCs became atrophic and spindle-shaped morphology with long hair-like actin fiber. No significant differences were found between the center-BRONJ GMSCs and peri-BRONJ GMSCs. The flow cytometry results (Fig. 3C) showed that these cells were all positive for mesenchymal stem cell (MSC)–related markers STRO-1, CD90, and CD105.

BRONJ GMSCs Exhibited poor proliferation, adhesion and migration ability than control GMSCs

The cell growth curves are illustrated in Fig. 3E. Compared with control GMSCs, the central and peripheral BRONJ GMSCs all showed a lower proliferation, but no significant differences were found between the center-BRONJ GMSCs and peri-BRONJ GMSCs. Figure 3D shows direct microscopic observation in cell migration. The capacities of cell migration in BRONJ GMSCs were significantly diminished (the average migration area in control GMSCs: 92.83%±1.04% vs. center-BRONJ GMSCs: 70.23%±8.38% and peri-BRONJ GMSCs: 68.05%±9.51%)(Fig. 3G). As evident from this analysis (Fig. 3F), the number of adherent cells was remarkably diminished both in the central and peripheral BRONJ GMSCs. These results suggested that the abilities of proliferation, adhesion, and migration in the central and peripheral BRONJ GMSCs were all remarkably decreased compared with controls, while there was no obvious difference between the center-BRONJ GMSCs and peri-BRONJ GMSCs.

BRONJ GMSCs were arrested cell cycle in G0/G1-phase and underwent early apoptosis compared with control GMSCs

The percentage of cells in each cell cycle phase was determined by flow cytometry. Results are depicted in Fig. 4A, the percentage of cells in G0/G1 phase was significantly increased in the central and peripheral BRONJ GMSCs compared with controls (Fig. 4C). Figure 4B shows the percentage of cell apoptosis in all groups. As evident from this analysis (Fig. 4D), in comparison with control GMSCs, center-BRONJ GMSCs showed the highest percentage of early apoptotic cells and peri-BRONJ GMSCs showed higher rate. Immunohistochemical staining showed remarkably increased expression of caspase 3 (the apoptotic executioner) in BRONJ gingival tissues (Fig. 2D). Apoptosis was also evaluated as the number of $TUNEL^+$ cells in different groups (Fig. 2E), similar levels of $TUNEL^+$ cells existed between the center and peripheral area of BRONJ lesions, but the apoptotic cells in BRONJ lesions were significantly higher than in healthy tissues. Taken together, these results indicated that the central and peripheral BRONJ GMSCs were all arrested cell cycle in G0/G1-phase and underwent early apoptosis compared with controls.

Bronj Gmscs Displayed Suppressed Expressions Of Tgf-β1 Signaling Pathway

GMSCs mRNA levels were determined by quantitative PCR. TGF-β1, Smad3 and COLIA1 were the most significantly downregulated both in the central and peripheral BRONJ GMSCs compared with controls, however, there was no statistical difference between the center-BRONJ GMSCs and peri-BRONJ GMSCs (Fig. 4E). The same pattern was further confirmed by western blot, which showed a lower expression of TGF-β1, p-Smad3 and COLIA1 both in the central and peripheral BRONJ GMSCs than that in the controls (Fig. 4F). Thus, we speculated that BRONJ GMSCs were associated with impaired gingival healing may via suppressing TGF-β1 signal pathway.

Bronj Gmscs Showed Significantly Lower Cell Viability In Vivo

The GFP fluorescence reached peak levels 72 h after lentiviral transduction in different groups (Fig. 6A). Hydrogel (20) laden with luciferase/GFP-labeled GMSCs were transplanted in skin healing model in nude mice to trace cell survival. Bioluminescence imaging (Fig. 6B) showed significant differences in different groups on days 5 and 14, performing significantly lower cell survival rate in BRONJ GMSCs groups than that in hydrogel/ control GMSCs group, while there was no statistical difference between the hydrogel/center-BRONJ GMSCs group and hydrogel/peri-BRONJ GMSCs group (Fig. 6C). When further investigating the samples by frozen sectioning and IF staining in excisional wound beds (Fig. 7C), we also found lower cell viability in BRONJ GMSCs groups than controls (Fig. 7D).

BRONJ GMSCs transplantation exhibited poor wound healing effect than that of control GMSCs in mice model

Given the essential role of GMSCs in gingival wound healing, we evaluated the wound healing effects of BRONJ GMSCs using an excisional skin healing model in nude mice. Figure 7A shows optical images of all groups at 0, 5, 10 and 14days post-surgery. The wound size of hydrogel/ control GMSCs group was the smallest compared to the other three groups, and the wounds had almost closed by 14 days. Both BRONJ GMSCs groups had a better repair effect than hydrogel alone group, while there was no statistical difference between the center-BRONJ GMSCs group and peri-BRONJ GMSCs group. Quantitation of the cutaneous wound size confirmed the above results (Fig. 7B). H&E staining showed the neo-epithelium in the cutaneous wound defects in all groups (Fig. 8A). The yellow line indicated the length without re-epithelialization in the wound. The total neo-epithelium in hydrogel alone group was the shortest compared with the other three groups. While the neo-epithelium length in hydrogel/ control GMSCs group was significantly longer than BRONJ GMSCs groups, there was no statistical difference between the center-BRONJ GMSCs group and peri-BRONJ GMSCs group (Fig. 8B). Masson’s staining (Fig. 8C) and quantitative analysis were applied to evaluate the collagen deposition and maturation. Extensive deposition of collagen fibers was observed in the wound bed of the hydrogel/ control GMSCs group compared with the other three groups. Quantitative analysis (Fig. 8D) revealed that the content of the collagen in hydrogel/ control GMSCs group was significantly higher than the other three groups, but there was no significant difference between the center-BRONJ GMSCs and peri-BRONJ GMSCs group.

To further explore the exact mechanism, IH staining of COLIA1, TGF-β1, Smad3 was performed to detect the fibrosis in the wound beds at 14days post-surgery (Fig. 8E). COLIA1, TGF-β1 and Smad3 were the most significantly downregulated in the center-BRONJ GMSCs and peri-BRONJ GMSCs groups compared with the controls, however, there was no significant difference between the center-BRONJ GMSCs and peri-BRONJ GMSCs group (Fig. 8F). Previously, BRONJ patients' gingival samples also confirmed the downregulated expression of COLIA1 and TGF-β1(Fig. 2D). Overall, these results suggested that BRONJ GMSCs transplantation exhibited poor wound healing effects in mice model than that of control GMSCs may via suppressing TGF-β1 signaling pathway. The schematic illustration was shown in Fig. 9.

Discussion

In this study, we successfully isolated GMSCs from BRONJ patients' gingiva, and demonstrated for the first time that BRONJ GMSCs showed decreased proliferation, adhesion, migration capacities and underwent early apoptosis in vitro compared with control GMSCs. Importantly, BRONJ GMSCs transplantation in a mice excisional skin model exhibited poor wound healing effects than that of control group may via suppressing TGF-β1 signaling pathway. Our findings highlight the decreased regeneration capacity of oral mucosa in BRONJ patients and provide new insights into the prevention of BRONJ by improving functions of BRONJ GMSCs in accelerating gingival wound healing.

The key clinical feature of BRONJ is the retarded gingival healing with necrosis exposure (24), however, it is still unclear why such the lesion should present with loss of oral soft tissue as the primary clinical feature. In present study, we found that BRONJ patients' gingiva appeared as disordered lamina propria and displayed notably depressed expressions of collagen. Despite a growing body of evidence demonstrated that BPs have direct toxic effect on oral soft tissue, however, the internal microenvironment of oral mucosa in BRONJ patients remains elusive. To better explore oral mucosa microenvironment, firstly, we performed an Affymetrix Gene Expression Array analysis feature using gingival tissues obtained from BRONJ patients or healthy people and explored differentially regulated genes. GO enrichment analysis showed that "negative regulation of wound healing" as one of the most significantly associated biological process in BRONJ lesions. KEGG analysis revealed that "TGF-β signaling pathways" as the significantly enriched functional pathway associated with the retarded gingival wound healing in BRONJ patients. Numerous studies have reported that TGF-β signaling pathway plays a crucial role in wound healing by controlling collagen synthesis (25–27). Combined with the above functional analysis, we speculated that BPs may through suppressing TGF-β signaling pathways inhibit collagen expression and delay gingival wound healing, ultimately leading to the development of BRONJ in cancer patients treated with intravenous BPs.

To verify the microarray results, we further assessed the expression of TGF-β signaling pathway in BRONJ patients' gingival tissues. RT-PCR showed that the mRNA levels of TGF-β1, Smad3, and COLIA1 but not TGF-β3, COL11A1 and Smad2 were remarkably decreased in BRONJ gingiva. Indeed, IH staining showed a lower expression of TGF-β1 and COLIA1 both in the central and peripheral area of BRONJ sites than that in healthy gingival tissues. TGF-β1 is a pleiotropic cytokine with a crucial role in mediating the

differentiation and proliferation of GMSCs and regulating the epithelial-to-mesenchymal transition during wound healing (28, 29), and Smad3 was identified as the downstream TGF-β1 effector (30, 31). TGF-β1 signaling pathway plays an important role in fibrosis. Briefly, TGF-β1 binding to TGF-β receptor leads to the phosphorylation of Smad2 and Smad3, and phosphorylated Smad2 and Smad3 subsequently form a complex, which translocates to the nucleus and interacts with nuclear transcription factors, where they regulate the transcription of specific fibrosis-related genes (26). Previous studies have reported that decreased TGF-β1 and Smad3 expression was shown to be related to delayed wound healing and impaired collagen deposition. Thus, the depressed expression of TGF-β1 signaling pathway might explain impaired gingival healing in BRONJ patients.

The oral gingiva as a unique soft tissue is superior in terms of preventing wound infection and promoting the underlying bone remodeling (32). Increasing evidence also supported that the gingival wound healing properties—rapid re-epithelialization, and fetal-like scarless healing—are driven primarily by GMSCs (8, 33). Previous studies have showed that BPs directly inhibited healthy GMSCs viability in vitro (5, 10, 11). However, to our knowledge, there was a lack of direct evidence that demonstrated the activities of GMSCs derived from BRONJ patients' gingiva as well as the roles of BRONJ GMSCs in impaired gingival healing. In this study, we successfully isolated GMSCs from the center area of BRONJ gingiva and peripheral area, and showed that they were positive for MSC related markers STRO-1, CD90, and CD105. They were all fibroblast-like cells, but the center-BRONJ GMSCs and peri-BRONJ GMSCs became slender and more wrinkled, resembling ice crystals. Consistent with the microscopic observation, the cytoskeletal stress fibers in the central and peripheral BRONJ GMSCs became atrophic and spindle-shaped morphology with long hair-like actin fiber under the fluorescence microscope. As we all know, the cytoskeletal stress fiber structure plays essential roles in cellular functions such as shape maintenance and active motility (34). On the basis of this observation, we speculated that the cellular functions in the central and peripheral BRONJ GMSCs must be impaired.

As expected, we demonstrated that the capabilities of proliferation, adhesion and migration in the central and peripheral BRONJ GMSCs all remarkably decreased compared with controls. Consistently, Y. Zhang et al. also reported the proliferative rate of BRONJ BMSCs from both the central and peripheral regions dramatically decreased (35). Our previous research using BRONJ periodontal tissue has demonstrated the increased expression of caspase 3 in BRONJ sites, especially in periodontal ligament (3). Similarly, in this study, we also observed the remarkably increased expression of caspase 3 in BRONJ gingiva. Apoptotic cells in BRONJ gingival tissues were also detected by TUNEL assay, we found that the apoptotic cells (TUNEL + cells) in the center area of BRONJ lesions and the peripheral area were all higher than in health gingiva. We further investigate cell cycle and apoptosis using flow cytometry and demonstrated that BRONJ GMSCs were arrested cell cycle in G0/G1-phase and underwent early apoptosis compared with controls. Therefore, we believed that retarded gingival healing in BRONJ patients might be related to the decreased capacities of cell proliferation, adhesion, migration and apoptosis in BRONJ GMSCs.

To further assess cell vitality and wound healing capacity in vivo, we transplanted BRONJ GMSCs with hydrogel into full-thickness wound sites of nude mice, which is the most commonly used animal model for excisional wound healing (17). Hydrogels are among the best options for wound dressing due to its high moisture retention capacity and excellent biomimetics properties similar to the extracellular matrix, which are preferable three-dimensional cell culture and can serve as a scaffold for GMSCs in contributing to wound healing (21). After hydrogel laden with luciferase/GFP-labeled BRONJ GMSCs were transplanted in mice excisional wound, bioluminescence imaging (36) traced cell survival and showed lower cell long-term survival rate in BRONJ groups than that in control group. These results were coordinated with previous in vitro results showing that the decreased capabilities of cell proliferation, adhesion and migration in BRONJ GMSCs. When analyzing the samples by frozen Sect. (37) and IF staining, we also found the consistent lower cell viability in BRONJ groups than. At 2weeks post-transplantation, the healing effect in the hydrogel/ control GMSCs group is the fastest compared with other three groups, both BRONJ GMSCs groups also had a better repair effect than hydrogel alone group. All mice were sacrificed after 2 weeks and then the samples were analyzed using H&E and Masson staining. As we expected, BRONJ GMSCs groups exhibited shorter re-epithelialization in the H&E staining and decreased collagen deposition in Masson analysis. According to these data, we can infer that 1) the application of GMSCs can effectively promote wound healing; 2) BRONJ GMSCs showed significantly lower cell viability in vivo; 3) BRONJ GMSCs transplantation in mice has poor effects on cutaneous wound healing compared with control GMSCs.

To investigate the exact mechanism of how BRONJ GMSCs transplantation delayed skin wound healing, BRONJ GMSCs mRNA levels were determined by quantitative PCR. Of note, TGF-β1, Smad3 and COLIA1 were the most significantly downregulated both in the central and peripheral BRONJ GMSCs. The same pattern was further confirmed by western blot. Moreover, the transplantation wound beds were also analyzed by IH staining to detect the fibrosis, and COLIA1, TGF-β1 and Smad3 were also significantly downregulated in BRONJ GMSCs groups. Overall, we found that the expression of TGF-β1 signaling pathway was suppressed not only in BRONJ patients' gingival lesions but also in BRONJ GMSCs transplantation animal model, which may be associated with the impaired gingival healing in BRONJ.

For the underlying mechanism of BRONJ, based on our results, we infer that the dysfunction of BRONJ GMSCs delayed gingival wound healing in BRONJ patients mainly via suppressing TGF-β1 signaling pathway, ultimately leading to the occurrence of BRONJ. In this process, several key points must be emphasized. First, cancer patients receive a ten-fold higher dosage of BPs than those with osteoporosis, under long-term BPs treatment, there is a direct cytotoxic effect on GMSCs by blood support as well as the BPs enriched underlying bone. The cellular functions and activities of GMSCs in BRONJ patients must be impaired. Second, GMSCs dysfunction have the negative influence on the re-epithelialization and the collagen deposition, and further delayed gingival wound healing. Third, retarded gingival healing led to the invasion of bacteria into the wound, contributing to inflammatory infiltration and the development of BRONJ.

Conclusions

In summary, we demonstrated for the first time the dysfunction of BRONJ GMSCs and that BRONJ GMSCs transplantation in a mice excisional skin model displayed poor effects on wound healing mainly via suppressing TGF-β1 signaling pathway. Because there are no available therapeutical approaches for BRONJ, improving the functions of BRONJ GMSCs and activating TGF-β1 signaling pathway may be therapeutically effective in managing BRONJ.

Abbreviations

BRONJ
Bisphosphonate-related osteonecrosis of the jaw BRONJ; BPs:bisphosphonates; GMSCs:gingival mesenchymal stem cells; GFP:green fluorescent proteins; RT-PCR:real-time polymerase chain reaction; COLIA1:collagen type I A1; TGF-β:transforming growth factor beta; GO:gene ontology; KEGG:kyoto encyclopedia of genes and genomes; PBS:phosphate buffered saline; MOI:multiplicity of infection; H&E:hematoxylin and eosin; DAPI:40,6-diamidino-2-phenylindole; TUNEL:terminal deoxynucleotidyl transferase-mediated dUTP-biotin nick end labeling assay; TRITC:Tetramethyl Rhodamine Isothiocynate; IH:immunohistochemistry; IF:immunofluorescence.

Declarations

Ethics approval and consent to participate

All research procedures were approved by the Ethics Committee of Shanghai Ninth People's Hospital (Number: SH9H-2020-T36-2), and written informed consent was obtained from all study participants. Animal experimental procedures were approved by the Experimental Animal Welfare and ethics branch of Shanghai Ninth People's Hospital (Number: SH9H-2020-A621-1), following the guidelines of the Laboratory Animal Manual of the NIH Guide to the Care and Use of Animals.

Consent for publication

Not applicable.

Availability of data and materials

All data included in this study are available upon request by contacting with the corresponding author.

Competing interests

The authors declare no potential conflicts of interest with respect to the authorship and publication of this article.

Funding

This work was supported by a grant from the National Natural Science Foundation of China (No. 81271114, 31700848 and 81200815), Shanghai Rising-star Program (20QA1405700) and Science and Technology Commission of Shanghai Municipality (19411962000, 17441902000 and 18441903000).

Authors' contributions

Mengyu Li carried out most of the experiments and drafted the manuscript. Yejia Yu contributed to data analysis and interpretation as well as critically revised the manuscript. Yuqiong Zhou and Yueqi Shi participated in the clinical sample collection. Wenjie Zhang and Jing Ge provided advice during the experimental design stage. Geehun Son participated in the animal experiments. Jun Zhao, Zhiyuan Zhang and Chi Yang contributed to the conception and design and critically revised the manuscript. Shaoyi Wang contributed to the conception, design, and data interpretation as well as critically revised the manuscript. All authors read and approved the final manuscript.

Acknowledgements

Not applicable.

Author details

1 Department of Oral Surgery, Shanghai Key Laboratory of Stomatology & Shanghai Research Institute of Stomatology, National Clinical Research Centre for Oral Diseases, Ninth People's Hospital, Shanghai Jiao Tong University School of Medicine, Shanghai, China. 2 Department of Prosthodontics, Shanghai Engineering Research Centre of Advanced Dental Technology and Materials, Shanghai Key Laboratory of Stomatology & Shanghai Research Institute of Stomatology, National Clinical Research Centre for Oral Diseases, Ninth People's Hospital, Shanghai Jiao Tong University School of Medicine, Shanghai, China. 3 Department of Orthodontics, Shanghai Key Laboratory of Stomatology & Shanghai Research Institute of Stomatology, National Clinical Research Centre for Oral Diseases, Ninth People's Hospital, Shanghai Jiao Tong University School of Medicine, Shanghai, China. 4 Department of Oral-maxillofacial Head and Neck Oncology, Shanghai Key Laboratory of Stomatology & Shanghai Research Institute of Stomatology, National Clinical Research Centre for Oral Diseases, Ninth People's Hospital, Shanghai Jiao Tong University School of Medicine, Shanghai, China.

References

1. Kishimoto H, Noguchi K, Takaoka K. Novel insight into the management of bisphosphonate-related osteonecrosis of the jaw (BRONJ). Jpn Dent Sci Rev. 2019;55(1):95–102.
2. Alsalleeh F, Keippel J, Adams L, Bavitz B. Bisphosphonate-associated osteonecrosis of jaw reoccurrence after methotrexate therapy: a case report. J Endod. 2014;40(9):1505–7.
3. Li M, Yu Y, Shi Y, Zhou Y, Zhang W, Hua H, et al. Decreased Osteogenic Ability of Periodontal Ligament Stem Cells Leading to Impaired Periodontal Tissue Repair in BRONJ Patients. Stem Cells Dev. 2020;29(3):156–68.

4. Belibasakis GN, Hajishengallis G. Advances in Oral Mucosal Immunity and the Microbiome. Adv Exp Med Biol. 2019;1197:1–9.
5. Kim RH, Lee RS, Williams D, Bae S, Woo J, Lieberman M, et al. Bisphosphonates induce senescence in normal human oral keratinocytes. J Dent Res. 2011;90(6):810–6.
6. Ristow O, Ruckschloss T, Bodem J, Berger M, Bodem E, Kargus S, et al. Double-layer closure techniques after bone surgery of medication-related osteonecrosis of the jaw - A single center cohort study. J Craniomaxillofac Surg. 2018;46(5):815–24.
7. Paulo S, Laranjo M, Abrantes AM, Casalta-Lopes J, Santos K, Goncalves AC, et al. Synthetic Calcium Phosphate Ceramics as a Potential Treatment for Bisphosphonate-Related Osteonecrosis of the Jaw. Materials (Basel). 2019;12(11).
8. Zhang QZ, Nguyen AL, Yu WH, Le AD. Human oral mucosa and gingiva: a unique reservoir for mesenchymal stem cells. J Dent Res. 2012;91(11):1011–8.
9. Taniguchi N, Osaki M, Onuma K, Ishikawa M, Ryoke K, Kodani I, et al. Bisphosphonate-induced reactive oxygen species inhibit proliferation and migration of oral fibroblasts: A pathogenesis of bisphosphonate-related osteonecrosis of the jaw. J Periodontol. 2020;91(7):947–55.
10. Komatsu Y, Ibi M, Chosa N, Kyakumoto S, Kamo M, Shibata T, et al. Zoledronic acid suppresses transforming growth factor-beta-induced fibrogenesis by human gingival fibroblasts. Int J Mol Med. 2016;38(1):139–47.
11. Manzano-Moreno FJ, Illescas-Montes R, Melguizo-Rodriguez L, Costela-Ruiz VJ, Garcia-Martinez O, Ruiz C, et al. Impact of bisphosphonates on the proliferation and gene expression of human fibroblasts. Int J Med Sci. 2019;16(12):1534–40.
12. Ikeda T, Kuraguchi J, Kogashiwa Y, Yokoi H, Satomi T, Kohno N. Successful treatment of bisphosphonate-related osteonecrosis of the jaw (BRONJ) patients with sitafloxacin: new strategies for the treatment of BRONJ. Bone. 2015;73:217–22.
13. Khan AA, Morrison A, Hanley DA, Felsenberg D, McCauley LK, O'Ryan F, et al. Diagnosis and management of osteonecrosis of the jaw: a systematic review and international consensus. J Bone Miner Res. 2015;30(1):3–23.
14. Diniz IM, Chen C, Ansari S, Zadeh HH, Moshaverinia M, Chee D, et al. Gingival Mesenchymal Stem Cell (GMSC) Delivery System Based on RGD-Coupled Alginate Hydrogel with Antimicrobial Properties: A Novel Treatment Modality for Peri-Implantitis. J Prosthodont. 2016;25(2):105–15.
15. Albadawi H, Haurani MJ, Oklu R, Trubiano JP, Laub PJ, Yoo HJ, et al. Differential effect of zoledronic acid on human vascular smooth muscle cells. J Surg Res. 2013;182(2):339–46.
16. Zhang M, Jiang F, Zhang X, Wang S, Jin Y, Zhang W, et al. The Effects of Platelet-Derived Growth Factor-BB on Human Dental Pulp Stem Cells Mediated Dentin-Pulp Complex Regeneration. Stem Cells Transl Med. 2017;6(12):2126–34.
17. Galiano RD, Michaels Jt, Dobryansky M, Levine JP, Gurtner GC. Quantitative and reproducible murine model of excisional wound healing. Wound Repair Regen. 2004;12(4):485–92.

18. Park SA, Covert J, Teixeira L, Motta MJ, DeRemer SL, Abbott NL, et al. Importance of defining experimental conditions in a mouse excisional wound model. Wound Repair Regen. 2015;23(2):251–61.
19. Chen L, Tredget EE, Liu C, Wu Y. Analysis of allogenicity of mesenchymal stem cells in engraftment and wound healing in mice. PLoS One. 2009;4(9):e7119.
20. Shi Q, Qian Z, Liu D, Sun J, Wang X, Liu H, et al. GMSC-Derived Exosomes Combined with a Chitosan/Silk Hydrogel Sponge Accelerates Wound Healing in a Diabetic Rat Skin Defect Model. Front Physiol. 2017;8:904.
21. Tang Y, Lin S, Yin S, Jiang F, Zhou M, Yang G, et al. In situ gas foaming based on magnesium particle degradation: A novel approach to fabricate injectable macroporous hydrogels. Biomaterials. 2020;232:119727.
22. Ashburner M, Ball CA, Blake JA, Botstein D, Butler H, Cherry JM, et al. Gene ontology: tool for the unification of biology. The Gene Ontology Consortium. Nat Genet. 2000;25(1):25–9.
23. Kanehisa M, Goto S, Kawashima S, Okuno Y, Hattori M. The KEGG resource for deciphering the genome. Nucleic Acids Res. 2004;32(Database issue):D277-80.
24. Hokugo A, Kanayama K, Sun S, Morinaga K, Sun Y, Wu Q, et al. Rescue bisphosphonate treatment of alveolar bone improves extraction socket healing and reduces osteonecrosis in zoledronate-treated mice. Bone. 2019;123:115–28.
25. Beanes SR, Dang C, Soo C, Ting K. Skin repair and scar formation: the central role of TGF-beta. Expert Rev Mol Med. 2003;5(8):1–22.
26. Miscianinov V, Martello A, Rose L, Parish E, Cathcart B, Mitic T, et al. MicroRNA-148b Targets the TGF-beta Pathway to Regulate Angiogenesis and Endothelial-to-Mesenchymal Transition during Skin Wound Healing. Mol Ther. 2018;26(8):1996–2007.
27. Lodyga M, Hinz B. TGF-beta1 - A truly transforming growth factor in fibrosis and immunity. Semin Cell Dev Biol. 2020;101:123–39.
28. Toshniwal P, Nguyen M, Guedin A, Viola H, Ho D, Kim Y, et al. TGF-beta-induced fibrotic stress increases G-quadruplex formation in human fibroblasts. FEBS Lett. 2019;593(22):3149–61.
29. Han N, Jia L, Su Y, Du J, Guo L, Luo Z, et al. Lactobacillus reuteri extracts promoted wound healing via PI3K/AKT/beta-catenin/TGFbeta1 pathway. Stem Cell Res Ther. 2019;10(1):243.
30. Li L, Zhang R, Yang H, Zhang D, Liu J, Li J, et al. GDF15 knockdown suppresses cervical cancer cell migration in vitro through the TGF-beta/Smad2/3/Snail1 pathway. FEBS Open Bio. 2020;10(12):2750–60.
31. Bandyopadhyay B, Fan J, Guan S, Li Y, Chen M, Woodley DT, et al. A "traffic control" role for TGFbeta3: orchestrating dermal and epidermal cell motility during wound healing. J Cell Biol. 2006;172(7):1093–105.
32. Turri A, Elgali I, Vazirisani F, Johansson A, Emanuelsson L, Dahlin C, et al. Guided bone regeneration is promoted by the molecular events in the membrane compartment. Biomaterials. 2016;84:167–83.

33. Treves-Manusevitz S, Hoz L, Rachima H, Montoya G, Tzur E, Vardimon A, et al. Stem cells of the lamina propria of human oral mucosa and gingiva develop into mineralized tissues in vivo. J Clin Periodontol. 2013;40(1):73–81.
34. Sato K, Adachi T, Matsuo M, Tomita Y. Quantitative evaluation of threshold fiber strain that induces reorganization of cytoskeletal actin fiber structure in osteoblastic cells. J Biomech. 2005;38(9):1895–901.
35. He LH, Xiao E, An JG, He Y, Chen S, Zhao L, et al. Role of Bone Marrow Stromal Cells in Impaired Bone Repair from BRONJ Osseous Lesions. J Dent Res. 2017;96(5):539–46.
36. Morciano G, Imamura H, Patergnani S, Pedriali G, Giorgi C, Pinton P. Measurement of ATP concentrations in mitochondria of living cells using luminescence and fluorescence approaches. Methods Cell Biol. 2020;155:199–219.
37. Aeffner F, Faelan C, Moore SA, Moody A, Black JC, Charleston JS, et al. Validation of a Muscle-Specific Tissue Image Analysis Tool for Quantitative Assessment of Dystrophin Staining in Frozen Muscle Biopsies. Arch Pathol Lab Med. 2019;143(2):197–205.

Figures

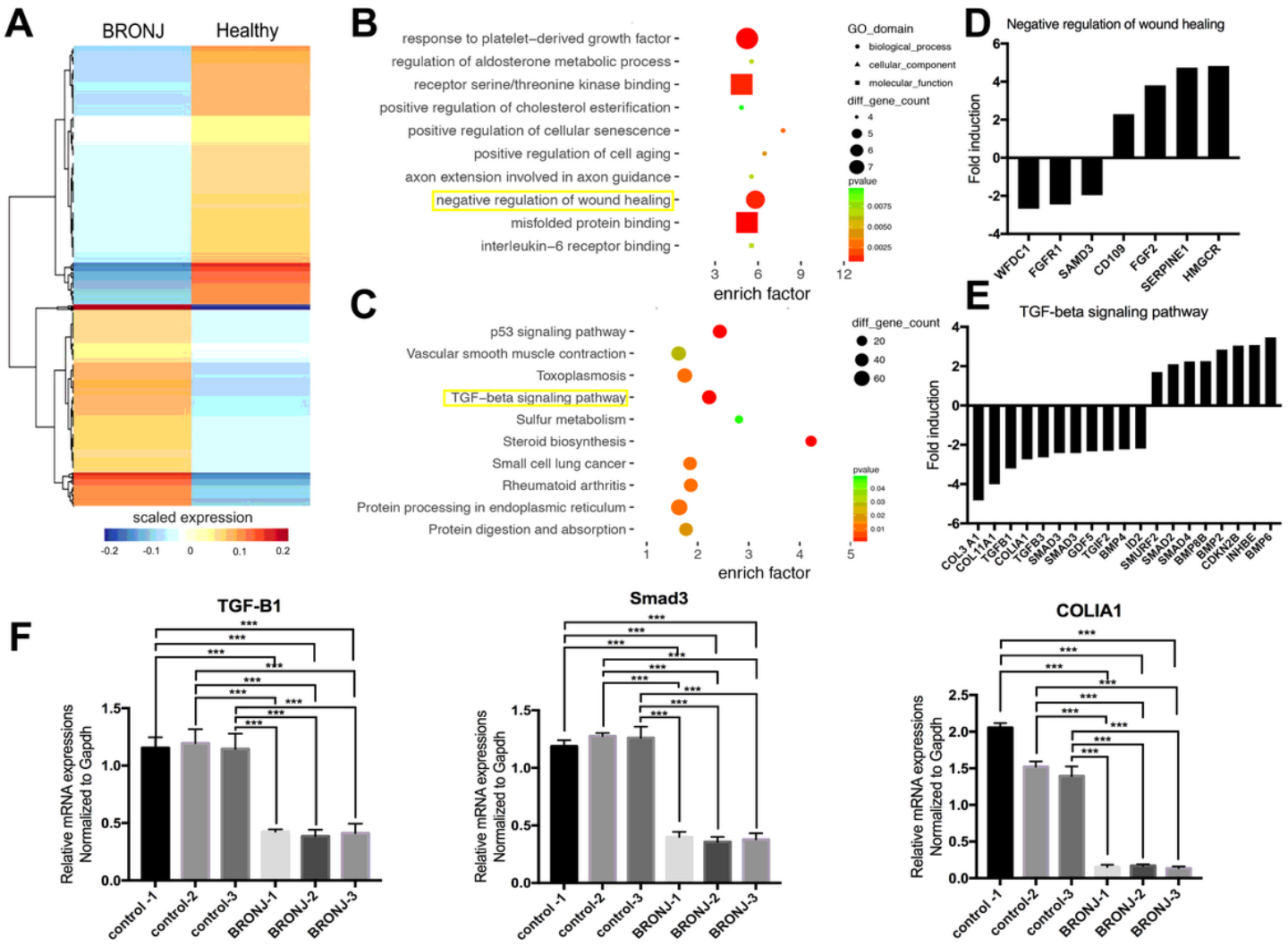

Figure 1

Microarray gene profiling identifies the activation of the negative regulation of wound healing and the suppressed TGF-β signaling pathways. (A) A graphic representation of the microarray profiling that are differentially expressed more than threefold were represented (n=3). (B) GO enrichment analysis identified “negative regulation of wound healing” as one of the most significantly associated biological process in BRONJ lesions. (C) Kyoto Encyclopedia of Genes and Genomes (KEGG) analysis showed “TGF-β signaling pathways” as the significantly enriched functional pathway associated with the retarded gingival wound healing in BRONJ patients. (D) Lists of genes involved in negative regulation of wound healing. (E) Lists of genes involved in TGF-β signaling pathways. (F) BRONJ gingival tissues and healthy gingiva were harvested and subjected to real-time PCR analysis. The results are from three different BRONJ patients and control people (***p < 0.001).

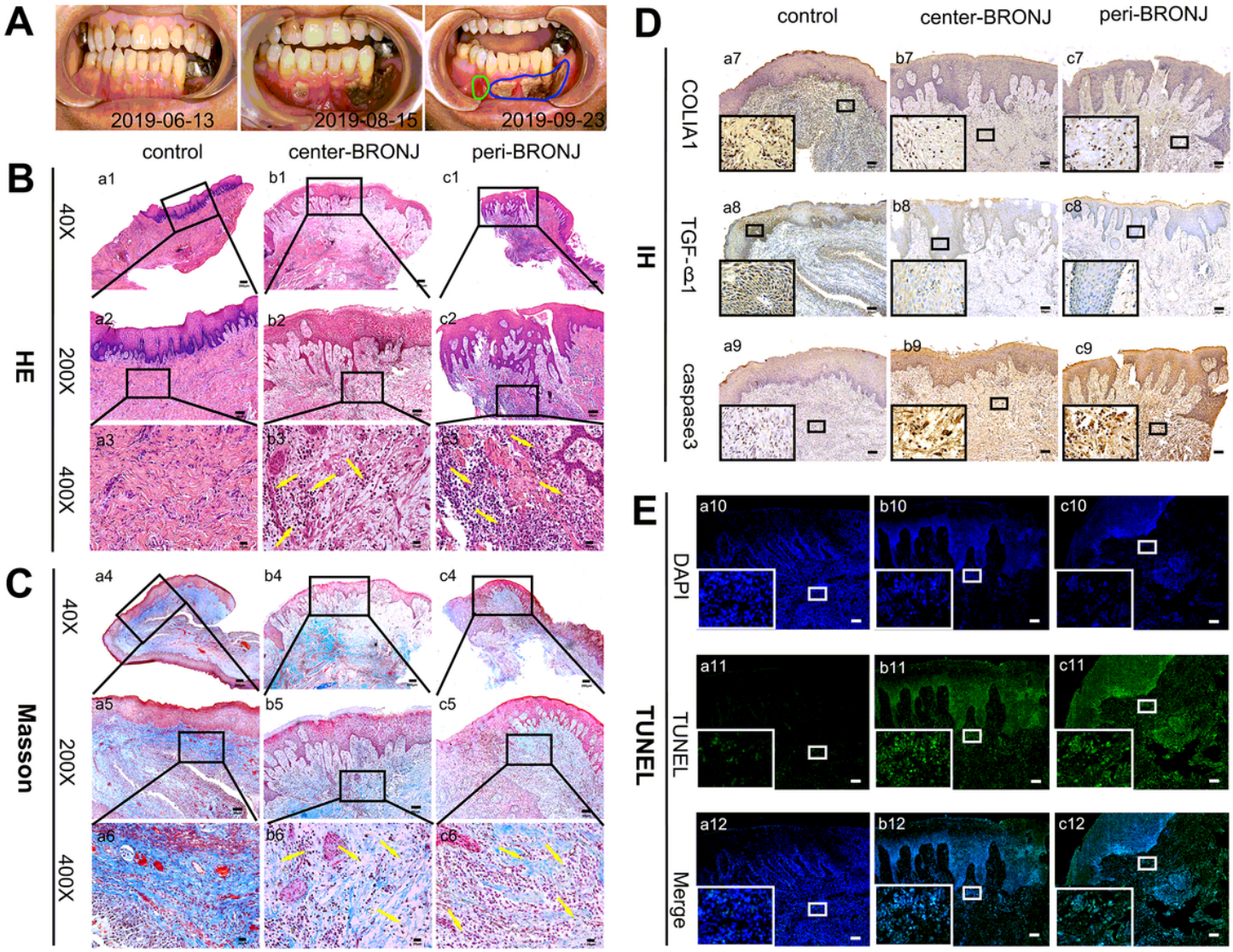

Figure 2

Histological analysis of gingival tissues from BRONJ patients and healthy people. (A) The progress of a BRONJ patient within 3 months, showing the progressive enlargement of the gingiva defect. The blue circle denotes the central area of BRONJ, and the green circle denotes the peripheral area from where the gingival samples were acquired and GMSCs were isolated. (B) Representative images of HE staining of gingival tissues in each group. (C) Masson staining of gingival tissues. (D) Immunohistochemical staining of COLIA1, TGF-β1 and caspase 3 in each group. (E) TUNEL staining of gingival samples in each group (a1–c1, a4–c4, bar = 200 μm; a2,5,7-12–c2,5,7-12, bar = 50 μm; a3–c3, a6–c6, bar = 20 μm).

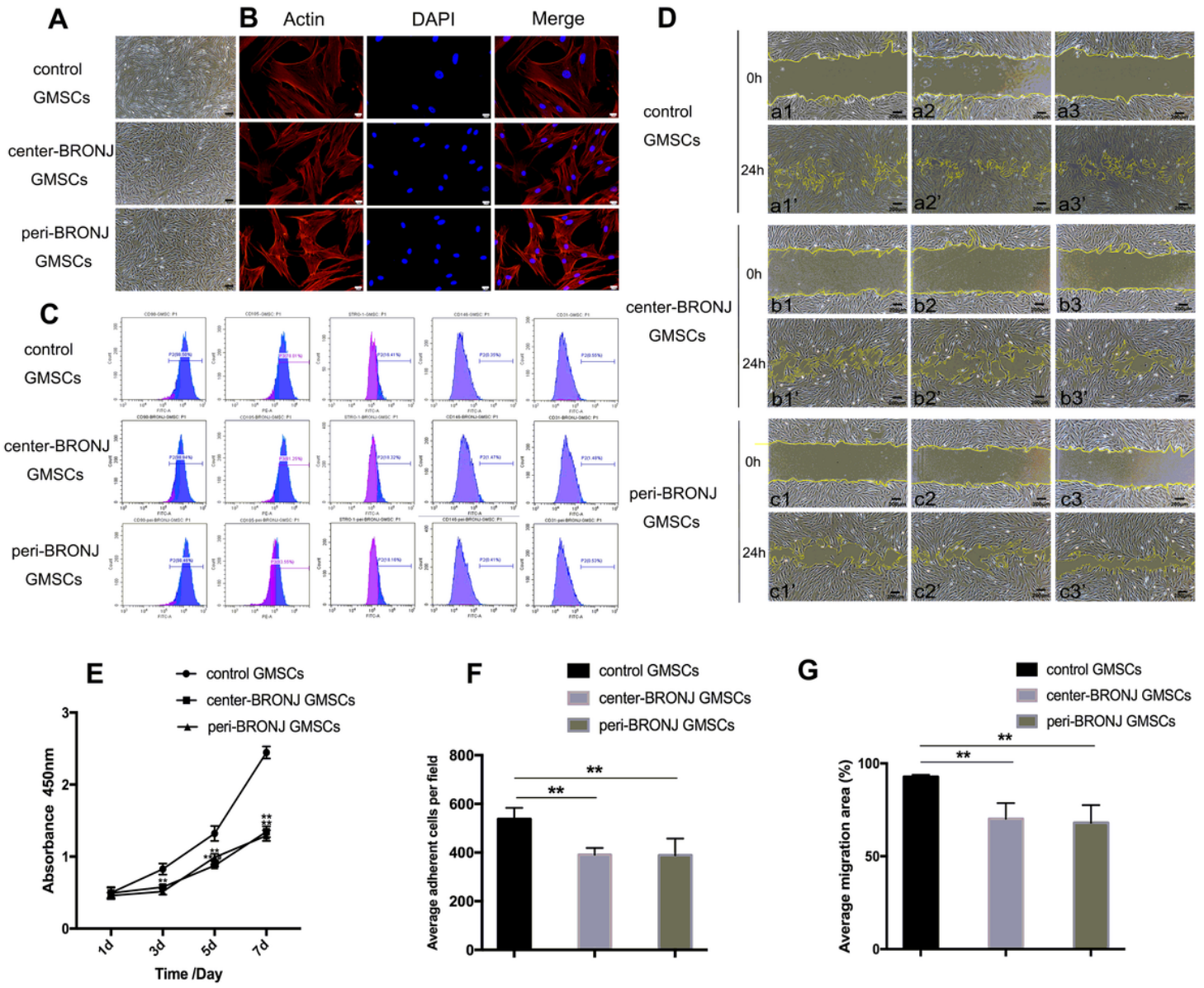

Figure 3

Isolation and identification of gingival marrow stem cells (GMSCs) from BRONJ patients' gingiva. (A) GMSCs derived from gingival tissues in the central area of the BRONJ region (center-BRONJ GMSCs), the peripheral area (peri-BRONJ GMSCs) and control patients (control GMSCs), respectively, were all fibroblast-like cells, but BRONJ GMSCs became slender and wrinkled, resembling ice crystals (Scale bar = 200μm). (B) Immunofluorescence assay for actin fiber evaluation (Scale bar = 20μm). (C) GMSCs identification by flow cytometry analysis. (D) Scratch wounds were directly microscopic observed at 0, 24 h. a1, a2, and a3 represent 3 different control patients. b1 and c1, b2 and c2, and b3 and c3 represent 3 BRONJ patients. The a, b, c represent the 0h images and a', b', c' represent the 24h images (Scale bar = 200μm). (E) Comparison of proliferative abilities of GMSCs were analyzed at 1–7 days. (F) Quantitative analysis of average adhesion cell count per field. (G) Quantitative evaluation of average migration area.

Data was represented as the mean ± SD from three independent experiments (*p < 0.05, **p < 0.01 and ***p < 0.001).

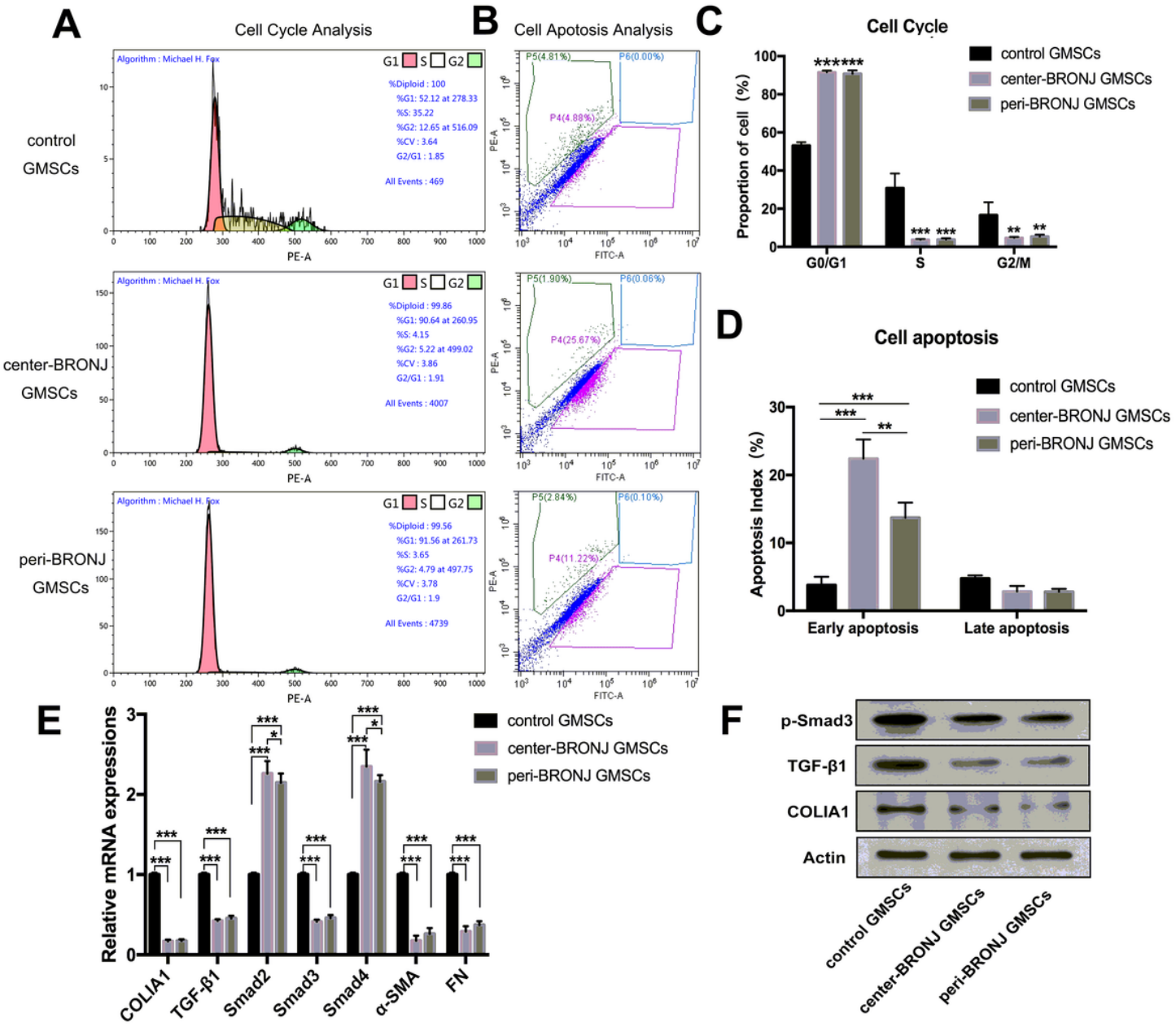

Figure 4

BRONJ GMSCs were arrested cell cycle in G0/G1-phase and underwent early apoptosis, and displayed lower expressions of TGF-β1, p-Smad3 and COLIA1. (A) Cell cycle and (B) apoptosis were determined by flow cytometric analysis in center-BRONJ GMSCs, peri-BRONJ GMSCs and control GMSCs. (C) Quantitative analysis of the percentage of GMSCs in each cycle phases and (D) the rate of early apoptotic cells in different groups. (**p < 0.01 and ***p < 0.001). (E) The mRNA levels of GMSCs in each groups were determined by real-time PCR. (F) Western blot showed the protein levels of TGF-β1, p-Smad3 and COLIA1 in GMSCs.

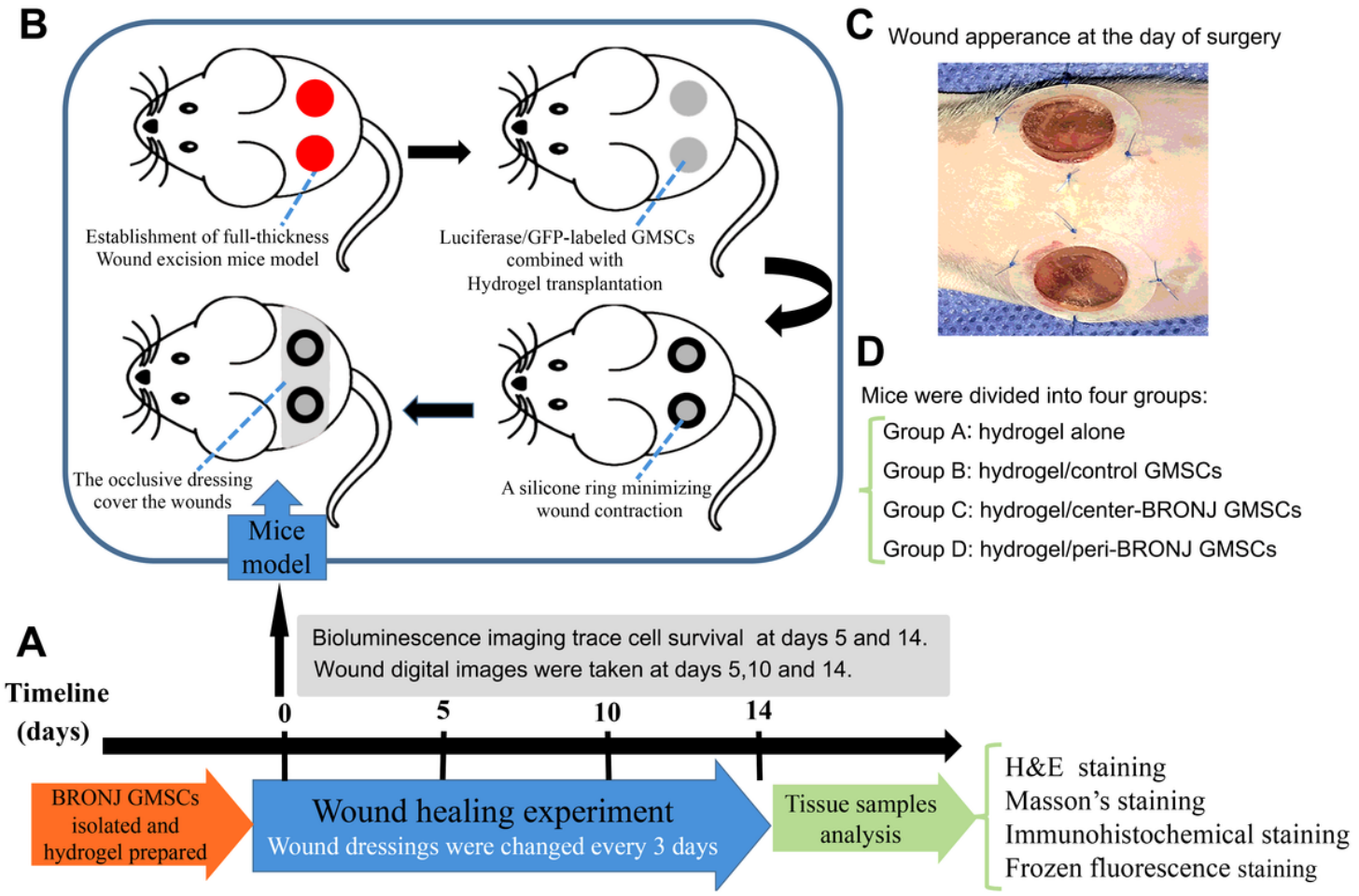

Figure 5

Animal experimental design for skin wound healing and the in vivo studies. (A) Timeline describing the in vitro cell isolated, hydrogel prepared and the mice wound healing experiment. (B) Building full-thickness excisional wound healing model and Luciferase/GFP-labeled GMSCs combined with hydrogel transplant into the wound site. (C) Wound appearance in mude mice at the day of surgery. (D) Mice were divided into four groups: Group A, hydrogel alone; Group B, hydrogel/control GMSCs; Group C, hydrogel/center-BRONJ GMSCs; Group D, hydrogel/peri-BRONJ GMSCs, n = 5.

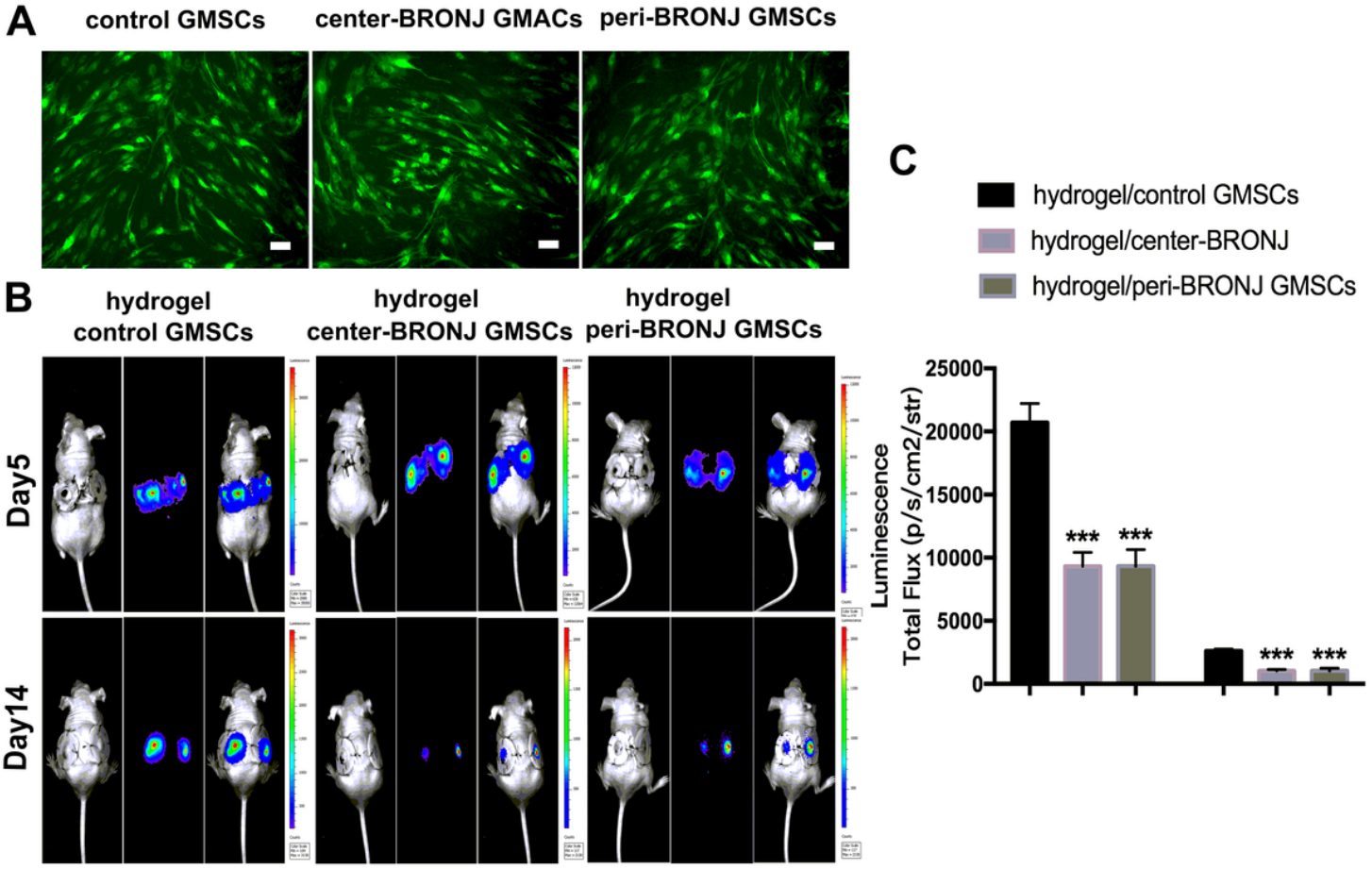

Figure 6

BRONJ GMSCs showed significantly lower cell viability in vivo. (A) Green fluorescent protein expression in GMSCs was observed after transduced by lenti-Luc/GFP. (B) The Luciferase/GFP-transduced GMSCs combined with hydrogel were transplanted in skin wound bed in mice. Cell viability and proliferation in vivo were measured by bioluminescence imaging on days 5 and 14. (C) Statistical analysis of the photon flux representing the viability of transplanted cells in mice (n = 5, ***p < 0.001, Scale bar = 50μm).

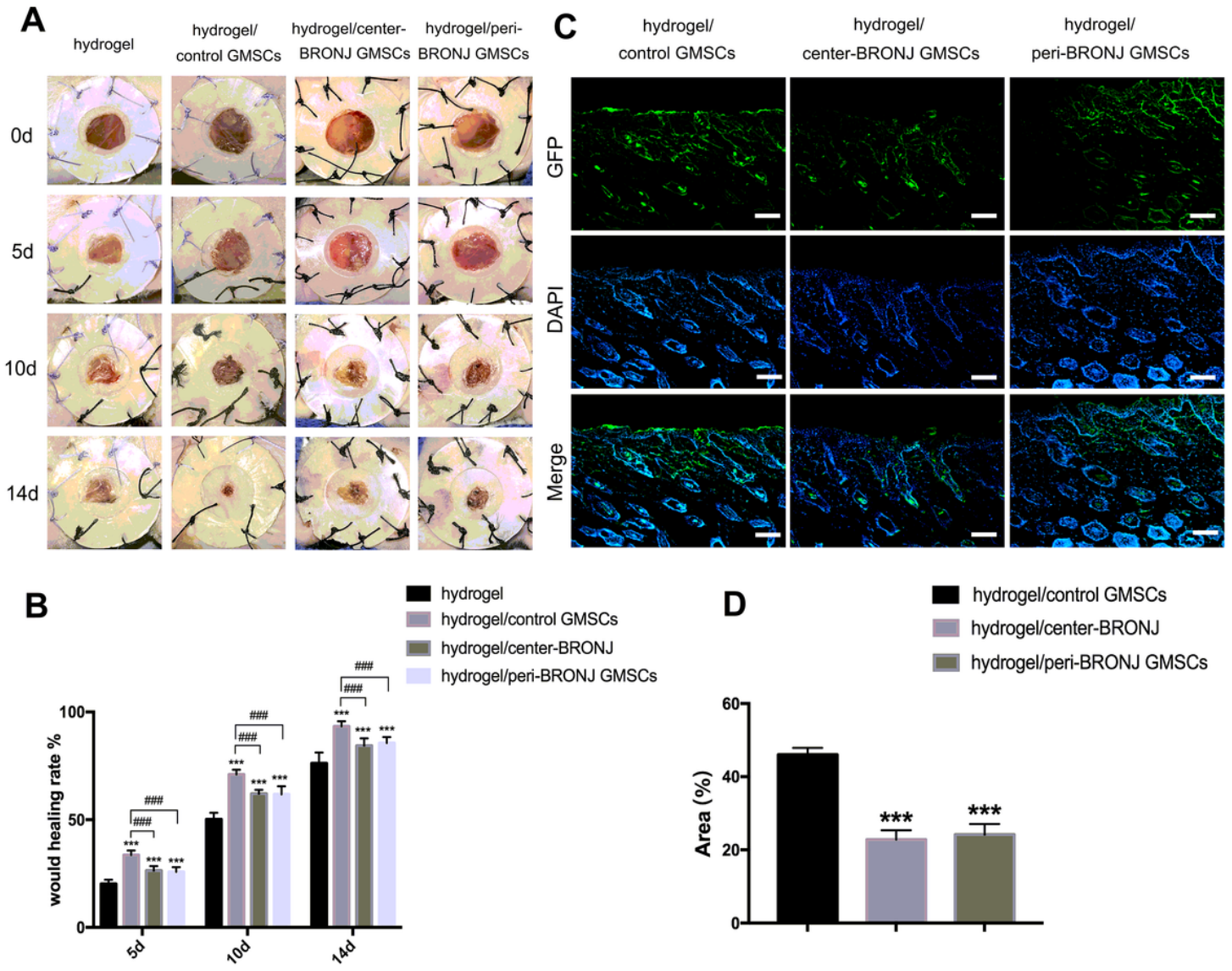

Figure 7

Macroscopic appearances and quantitative analysis of cutaneous wounds in the different groups. (A) Representative images of full-thickness skin defects in nude and quantitative analysis of the wound closure rates at 0, 5, 10 and 14 d post-surgery of hydrogel alone group, hydrogel/control GMSCs group, hydrogel/center-BRONJ GMSCs and hydrogel/peri-BRONJ GMSCs group. (B) Quantitative analysis of the wound healing rates in each group at 5, 10 and 14days post-surgery (n = 5, ***p < 0.001 compared to hydrogel alone group; ###p < 0.001 compared to the hydrogel/control GMSCs group). (C) Frozen sectioning and IF staining of cutaneous wound samples extracted on day 14. (D) Statistical analysis of GFP signal areas was based on 5 randomly selected high-power fields representing the viability of transplanted cells (n = 5, ***p < 0.001, Scale bar = 50μm).

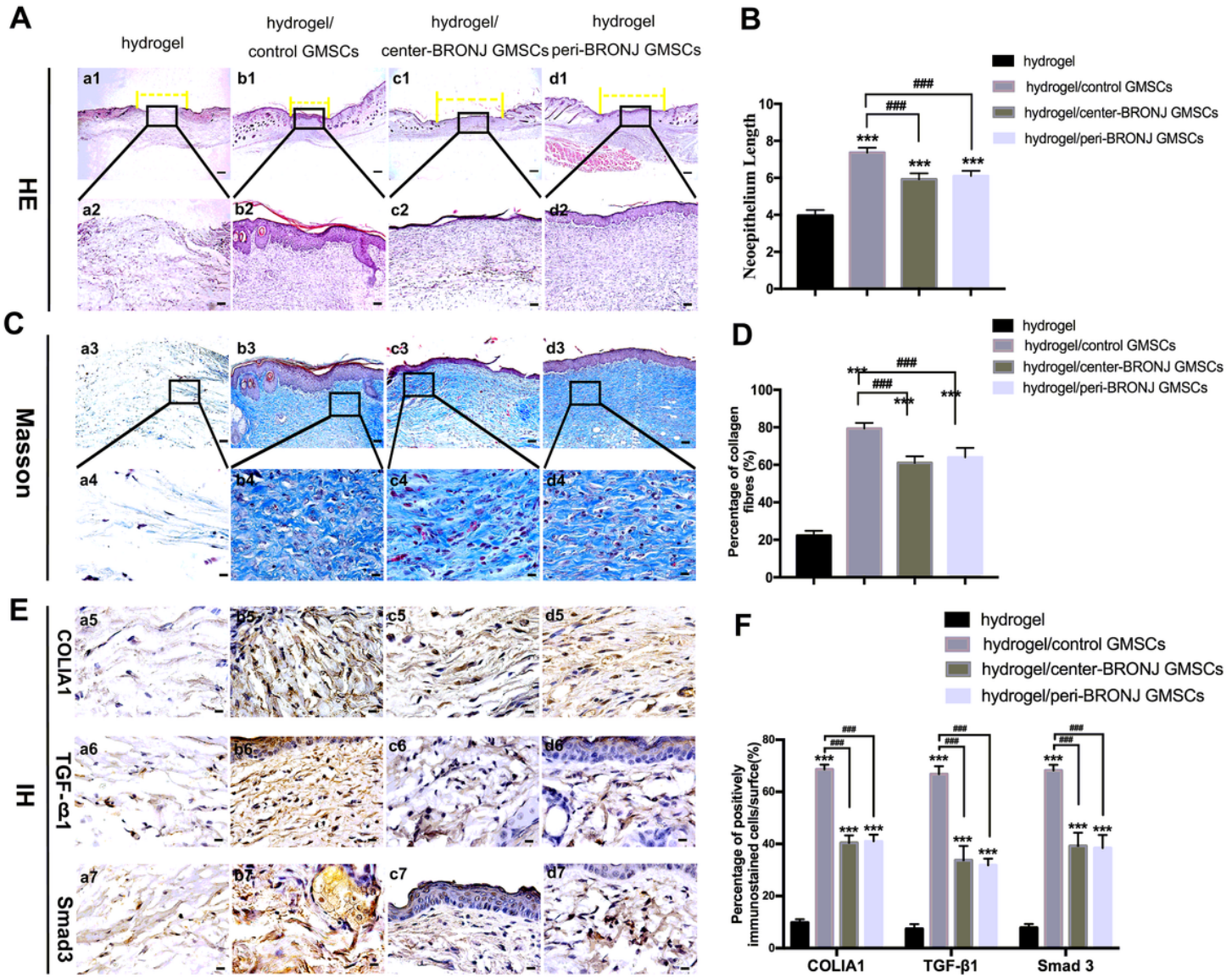

Figure 8

Histologic analysis of the wound sections. (A) Representative images of H&E staining of the wound sections in each group. The yellow dotted line indicates the length without re-epithelialization in the wound. (B) Quantitative analysis of the neo epithelialization in the four groups at 14d post-surgery. (C) Representative images of Masson staining of the wound sections in each group. (D) Quantitative analysis of the percentage of collagen in each group. (E) Immunohistochemistry to detect COLIA1, TGF-β1, Smad3 expressions in each group and (F) quantitative analysis of their expressions in the cutaneous wound beds (n = 5, ***p < 0.001 compared to hydrogel alone group; ###p < 0.001 compared to the hydrogel/control GMSCs group, a1–d1, bar = 200 μm; a2–d2, a3–d3, bar = 50 μm; c4-7–d4-7, bar = 10 μm).

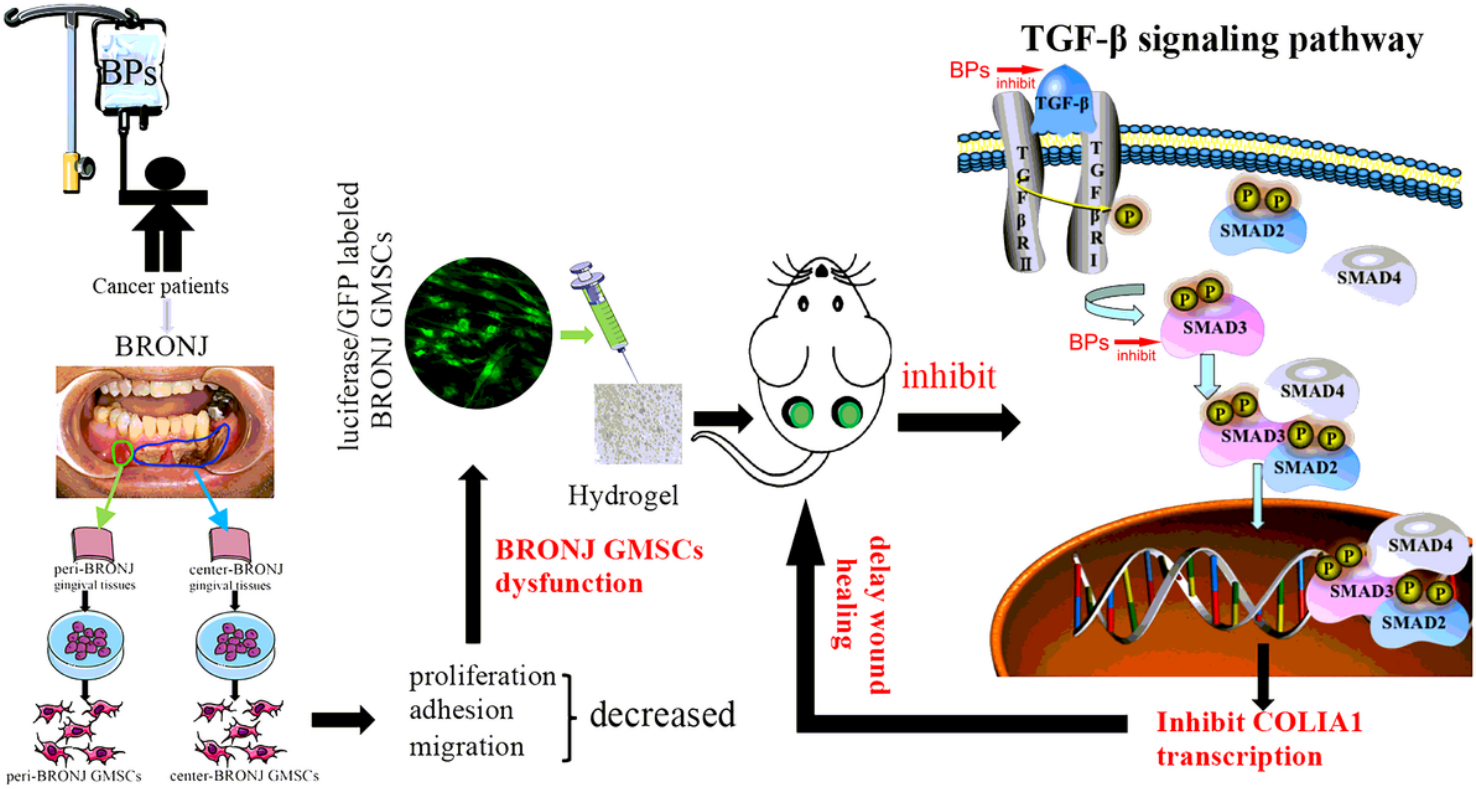

Figure 9

Schematic illustration of BRONJ GMSCs transplantation in a mice skin model delaying cutaneous wound healing mainly via suppressing TGF-β1 signaling pathway.

Supplementary Files

This is a list of supplementary files associated with this preprint. Click to download.

- Supplementfile.docx